# RIPPLE FORMATION AND WHOLE-PROCESS MODELLING OF SELECTIVE LASER MELTING

ZEKUN WANG[1], KHURAM WALAYAT[2], MOUBIN LIU[3]
[1] *BIC-ESAT & State Key Laboratory for Turbulence and Complex Systems, College of Engineering, Peking University, Beijing 100187, China, zekunwang@pku.edu.cn*
[2] *BIC-ESAT & State Key Laboratory for Turbulence and Complex Systems, College of Engineering, Peking University, Beijing 100187, China, khuram_walayat@yahoo.com*
[3] *BIC-ESAT & State Key Laboratory for Turbulence and Complex Systems, College of Engineering, Peking University, Beijing 100187, China, mbliu@pku.edu.cn*

***Keywords:*** *Ripples, Selective laser melting, Phase change, Marangoni flow, Whole-process modelling, OpenFOAM*

[Abstract] In this paper, we present the development of a modelling framework to simulate the powder deposition and powder melting with multiple tracks and multiple layers in selective laser melting (SLM). The framework is implemented through coupling the Finite Volume Method (FVM) and the Discrete Element Method (DEM). The framework is further used to investigate the ripple formation in SLM and a dimensionless number is then given to characterize the strength of ripple effects.

## Introduction

Selective laser melting (SLM) based on metal powders is a promising additive manufacturing technology which has already drawn attention in many industrial fields, e.g., aerospace engineering, bio-implants, smart materials and even architectures. However, the extremely intense laser hinders direct observation of the laser-powder interaction, making numerical simulation a powerful tool to explore the underlying physics like melting, balling, splashing and rippling.

During past decades, many researchers conducted numerical study on the melting process of the powder bed. Qiu et al. [1] and Panwisawas et al. [2] established a VOF-based frame to reproduce the melting process and the evolution of a single molten track. Khairallah et al. [3, 4] also provided comparable simulations results of the melting process in SLM and the formation mechanisms of pores, spatter, and denudation zones were also studied. Yan et al. [5] used Flow3D, EDEM and other commercial software and established a framework to reproduce the whole-process of electron beam selective melting (EBSM).

Surface roughness and the ripples that occur in SLM play important roles in product quality and reflectivity. Due to limited experimental conditions, it is difficult to figure out the detailed formation process of the surficial cavities and ripples, therefore, relevant studies are also conducted. Gečys et al. [6] studied the influence of laser frequency on the ripple formation. Besides, when laser power increases, the temperature gradient becomes lager, and the difference in surface tension drives the molten metal to a certain direction, namely, Marangoni effect. Kou et. al [7] studied this thermo-capillary force in welding and found that the content of surface-active agents will change the temperature dependence of the surface tension coefficient, thus affects the surface deformation. When the content of surface-active agent is low, the surface tension coefficient tends to be negative, and Marangoni force drives the molten liquid outward, and ripples occur where disturbance exists. However, the heat source in this study is fixed, thus ripples form a series of homocentric circles.

In this study, we coupled the Finite Volume Method (FVM) in *OpenFOAM* with Discrete Element Method (DEM) in *LIGGGHTS* to reproduce powder deposition. Thus the radii of the powders can be controlled as wished, e.g., Gaussian distribution. Then we modified the Volume of Fluid (VOF) solvers in *OpenFOAM* to reproduce the melting process during SLM, and the two-phase interface is reconstructed using a sharp interface capturing method, iso-Advector. Combining these two steps, we can simulate multi-track and multi-layer SLM with different powder distribution. In this paper, we also proposed a dimensionless number judging whether the ripples can occur, which considers the physical parameter of the material and laser beam, temperature gradient and powder bed morphology. Several simulations are performed and comparable results are obtained.

## Formulations and modelling processes

Deposition of the metallic powders are simulated by coupling *OpenFOAM* with *LIGGGHTS*, the governing equations for the powders are:

$$m_{pj}\frac{d\mathbf{V}_j}{dt} = -V_{pj}\nabla p + \mathbf{F}_{drag} + m_{pj}\mathbf{g} + \Sigma\mathbf{F}_{p-p} + \Sigma\mathbf{F}_{p-w} \tag{1}$$

$$\mathbf{I}_{pj}\frac{d\boldsymbol{\omega}_j}{dt} = \Sigma\mathbf{M}_t + \mathbf{M}_r \tag{2}$$

where $\mathbf{V}_j$, $m_{pj}$, $V_{pj}$ and $\mathbf{I}_{pj}$ are the velocity, mass, volume and rotational inertia of Particle *j*, respectively. *p* is the ambient pressure of air, and $\mathbf{g}$ is the gravitational acceleration. $\mathbf{F}_{drag}$ is the drag force exerted on the particle by surrounding air [8]. $\mathbf{F}_{p\text{-}p}$ is the particle-particle interaction force, and $\mathbf{F}_{p\text{-}w}$ is the particle-wall interaction forces while relevant details can be found in [9, 10]; $\mathbf{M}_t$ is the moment generated by tangential forces exerted by other particles and $\mathbf{M}_r$ is the rolling friction toque [11].

During the former DEM step, the drag force, position and velocity of a powder particle are calculated, and the information is sent to the CFD solver to calculate the momentum exchange. The governing equations for the CFD solver are the continuity equation and N-S equation:

$$\frac{\partial\alpha_I}{\partial t} + \nabla\cdot(\alpha_I\mathbf{V}_I) = 0 \tag{3}$$

$$\frac{\partial}{\partial t}(\alpha_I\rho_2\mathbf{V}_I) + \nabla\cdot(\alpha_I\rho_2\mathbf{V}_I\otimes\mathbf{V}_I) = -\alpha_I\nabla p - \nabla\cdot(\alpha_I\mu_2(\nabla\mathbf{V}_I)) + \alpha_I\rho_2\mathbf{g} - \frac{1}{V_{\mathrm{Cell}I}}\sum_{\forall j\in\mathrm{Cell}I}\frac{V_{pj}\beta(\mathbf{V}_I-\mathbf{V}_j)}{\alpha_{pj}}D(\mathbf{r}_I-\mathbf{r}_j) \tag{4}$$

where $\mathbf{V}_I$ and $\alpha_I$ are the velocity and volume fraction of air in cell *I*. $\rho_2$ and $\mu_2$ are the density and dynamic viscosity of air as the second phase. The last term is the source term that governs the momentum exchanges, in which $V_{\mathrm{Cell}I}$ is the volume of the air cell, $\beta$ is an empirical coefficient related to the particle void fraction $\alpha_{pj}$ of Cell *I* and Reynolds number, $\mathbf{r}_j$ is the position vector of the particles, $\mathbf{r}_I$ is that of air cell *I*, *D* is a distribution function that distributes the reaction forces on fluid phase at the velocity nodes in staggered Eulerian grids [12].

By now, the deposition of the powders can be reproduced. In order to simulate the melting process of the powder bed, the particles have to be 'moved' to FVM cells, and then we use VOF to distinguish metal phase from air phase, use iso-Advector [13] to reconstruct the interface. In VOF, metal phase is defined as the first phase $\alpha_1$, and the air as the second $\alpha_2$, $\alpha_1+\alpha_2=1$. Physical parameters are also weighed by the volume fractions, e.g., the viscosity $\mu=\alpha_1\mu_1+\alpha_2\mu_2$, where $\mu_1$ is the metallic viscosity, subscript 1 denotes the first phase, as with other parameters, which are not listed here. For convenience, $\alpha_1$ is just denoted as $\alpha$. Particle positions and theirs radii are obtained from the DEM solver, then we use *funkySetFields* tool in *swak4foam* to set the volume fraction according to the positions and radii. In the modified VOF solver, the governing equations are continuity equation, like Eqn.3, N-S equation and energy equation. N-S equation is written as:

$$\frac{d}{dt}(\rho\mathbf{U}) + \nabla\cdot(\rho\mathbf{U}\otimes\mathbf{U}) = \nabla\cdot(\mu\nabla\mathbf{U}) + c\kappa\nabla\alpha - \nabla p + \rho\mathbf{g} + \left|\nabla\alpha\right|\frac{\partial\kappa}{\partial T}(\nabla T - \mathbf{n}(\mathbf{n}\cdot\nabla T)) \tag{5}$$

where $\mathbf{U}$ is velocity, *t* is time, $\rho$ is density, $\mu$ is viscosity, in particular, the viscosity of the molten metal $\mu_1$ is approximated by: $\ln\mu_1 = \frac{1}{2}\mathrm{erfc}[\frac{4}{\ln T_l - \ln T_s}\cdot(\ln T - \frac{\ln T_s+\ln T_l}{2})](\ln\mu_s - \ln\mu_l) + \ln\mu_l$, where $T_l$ and $T_s$ are the liquidus and solidus point, $\mu_s$ and $\mu_l$ are the viscosity of solid and liquid metal. And *c* is the curvature, $\kappa$ is the coefficient of surface tension, *p* is pressure, $\mathbf{g}$ is gravitational acceleration, *T* is temperature.

Energy equation is:

$$\frac{d}{dt}(\rho CT + \rho L\alpha_m) + \nabla\cdot(\rho CT\mathbf{U} + \rho L\alpha_m\mathbf{U}) - \nabla\cdot\nabla(kT) = -\left|\nabla\alpha\right|[h_c(T-T_{ref}) - \frac{2\eta P}{\pi R^2}\exp(\frac{-2\left|\mathbf{x}-\mathbf{X}_l(t)\right|^2}{R^2})] + \Phi, \tag{6}$$

where *C* is thermal capacity, *L* is latent heat of fusion, $\alpha_m$ is melting degree, $\alpha_m = \frac{1}{2}[1+\mathrm{erf}(\frac{4}{T_l-T_s}(T-\frac{T_l+T_s}{2}))]$, *k* is thermal conductivity, $h_c$ is heat transfer coefficient, $T_{ref}$ is the reference temperature, *P* is the laser power, $\eta$ is

laser absorption coefficient, $R$ is the effective laser beam radius, **x** is the position vector of a FVM cell, **X** is the laser scanning path and $\Phi$ is the dissipation.

Last but not the least, we use iso-Advector to reconstruct the surface of the first layer of powder bed and export it using *Paraview* in *stl* files. The *stl* files are then imported to *LIGGGHTS* and set as boundary condition for another round of powder deposition. Accordingly, the SLM process of the succeeding layer of powder bed can again be reproduced by the aforementioned steps. Figure 1 shows the simulation results of the molten track on the first layer of powder bed, and Figure 2 shows the deposition of the succeeding layer on the original layer.

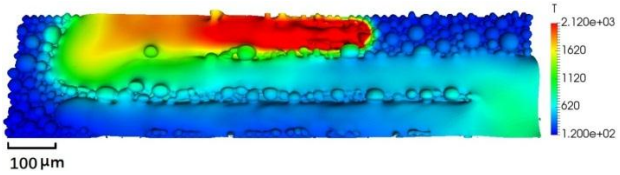


**Figure 1: Molten track on the first layer of powders.**

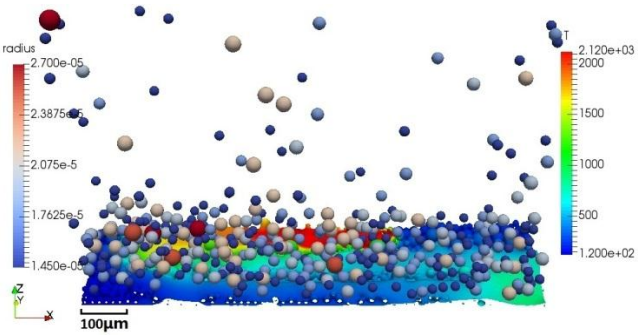


**Figure 2: Deposition of powders for the succeeding layer.**

**Ripple formation**

Ripples that formed during SLM has great influence on the surface structure and reflectivity of the product, and the ripple marks between layers could evolve into cracks and break the structure under fatigue loading. Hence, studies on rippling and its wavelength should claim more attention.

There are several characteristic velocities in SLM process: Molecular diffusion velocity $\frac{\nu_1}{R}$, where $\nu_1$ is the metallic kinematic viscosity; Thermal diffusion velocity $\frac{\alpha_1}{R}$, where $\alpha_1$ is the metallic thermal diffusivity; Characteristic velocities of surface tension and Marangoni force, $\sqrt{\frac{\kappa}{\rho_1 r}}$ and $\sqrt{\frac{\frac{\partial \kappa}{\partial T}(T_v - T_s)}{\rho_1 L_{v-s}}}$, respectively, where $r$ is the mean radius of particle, which is the distance for surface tension to smooth the surface, $T_v$ is the evaporation point and $L_{v-s}$ is the distance between laser spot and solidus line along the scanning path, where Marangoni flow exists. By comparison, it is easy to find that the last two velocities are pre-dominant during melting. In order to see whether the gaps between particles will be smoothed by the uniform part of surface tension or be stretched by Marangoni force and forms ripples, a ratio of these two characteristic velocities is given as $\theta = \sqrt{\frac{\kappa}{\frac{\partial \kappa}{\partial T}(T_v - T_s)} \frac{L_{v-s}}{r}}$.

Several simulations are conducted to see how the relevant physical parameters can influence this ratio. As shown in Figure 3 (a), (b) and (c), the particle radius is 9.8 $\mu m$, and temperature gradient or $\frac{\partial \kappa}{\partial T}$ increases. The particle radius in figure (d), (e) and (f) is 14 $\mu m$, and other parameters corresponds to (a), (b) and (c).

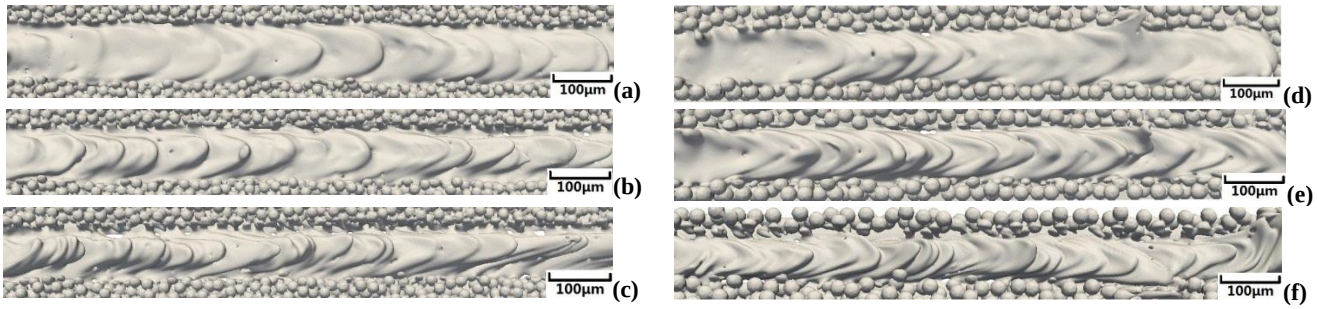


**Figure 3: Simulation results for different physical parameters. $\theta$ for figure (a), (b), (c) and (d), (e), (f) are 8.25, 5.04, 3.52, and 6.90, 3.43, 2.94..**

According to simulation results, if $\theta$ is larger than 8.25, rippling is very weak, and even vanishes as $\theta$ continue to grow. If $\theta$ is lower than 8.25, there exist two kinds of ripples. Ripples with long wavelength are dominant in Figure 3 (a), (b) and (d), where $\theta$ is larger than 5.04. However, in Figure 3 (c), (e) and (f), both ripples with short wavelength and long wavelength exist, where $\theta$ is lower than 5.04, and the ripples with short wavelength is believed to be caused by the gaps between particles.

**Conclusion**

In this work, we developed a modelling framework based on *OpenFOAM* and *LIGGGHTS* to reproduce the powder deposition and melting process of SLM. In industry, it is not easy to manipulate the material properties of the metals used in SLM, and this poses challenges to the study of many crucial physics inherent in SLM. However, with this modelling framework, we can freely change the physical parameters to study crucial physics in SLM like rippling, balling, splashing and so on. Additionally, both *OpenFOAM* and *LIGGGHTS* are open source codes, allowing us to develop more reliable physical models for better understanding and optimizing the manufacturing process in SLM.

**Acknowledgements**

We acknowledge the support by the Beijing Innovation Center for Engineering Science and Advanced Technology (BIC-ESAT), and the National Natural Science Foundation of China (NSFC) (Grant Nos. U1530110 and 51779003). The simulations have been conducted at Tianhe II Super Computer in the National Supercomputing Center in Guangzhou with the effective support from Beijing Paratera Technology Co., Ltd.

**References**

[1] C. L. Qiu, C. Panwisawas, M. Ward, H. C. Basoalto, J. W. Brooks, and M. M. Attallah, "On the role of melt flow into the surface structure and porosity development during selective laser melting," *Acta Mater.,* vol. 96, pp. 72-79, 2015.

[2] C. Panwisawas, C. L. Qiu, Y. Sovani, J. W. Brooks, M. M. Attallah, and H. C. Basoalto, "On the role of thermal fluid dynamics into the evolution of porosity during selective laser melting," *Scripta Mater. ,* vol. 105, pp. 14-17, 2015.

[3] S. A. Khairallah, A. T. Anderson, A. Rubenchik, and W. E. King, "Laser powder-bed fusion additive manufacturing: Physics of complex melt flow and formation mechanisms of pores, spatter, and denudation zones," *Acta Mater.,* vol. 108, pp. 36-45, 2016.

[4] W. King, A. T. Anderson, R. M. Ferencz, N. E. Hodge, C. Kamath, and S. A. Khairallah, "Overview of modelling and simulation of metal powder bed fusion process at Lawrence Livermore National Laboratory," *Mater. Sci. & Tech.,* vol. 31, no. 8, pp. 957-968, 2015.

[5] W. T. Yan *et al.*, "Multi-physics modeling of single/multiple-track defect mechanisms in electron beam selective melting," *Acta Mater.,* vol. 134, pp. 324-333, 2017.

[6] P. Gečys, "Ripple Formation by Femtosecond Laser Pulses for Enhanced Absorptance of Stainless Steel," *J Laser Micro Nanoen,* vol. 10, no. 2, pp. 129-133, 2015.

[7] S. Kou, C. Limmaneevichitr, and P. S. Wei, "Oscillatory Marangoni flow: A fundamental study by conduction-mode laser spot welding," *Weld. J.,* vol. 90, no. 12, pp. 229-240, 2011.

[8] S. Benyahia, M. Syamlal, and T. J. O'Brien, "Extension of Hill Koch Ladd drag correlation over all ranges of Reynolds number and solids volume fractions," *Powder. Technol.,* no. 162, pp. 166-174, 2006.

[9] A. D. Renzo and F. P. D. Maio, "Comparison Of Contact Force Models For The Simulation Of Collisions In DEM Based Granular Flow Codes," *Chem. Eng. Sci.,* vol. 59, no. 3, pp. 525-541, 2004.

[10] A. B. Stevens and C. M. Hrenya, "Comparison of soft-sphere models to measurements of collision properties during normal impacts," *Powder. Technol.,* vol. 154, no. 2-3, pp. 99–109, 2005.

[11] H. P. Zhu, Z. Y. Zhou, R. Y. Yang, and A. B. Yu, "Discrete particle simulation of particulate systems: Theoretical developments," *Chem. Eng. Sci.,* vol. 62, no. 13, pp. 3378-3396, 2007.

[12] R. J. Hill, D. L. Koch, and A. J. C. Ladd, "The first effects of fluid inertia on flows in ordered and random arrays of spheres," *J. Fluid Mech.,* vol. 448, pp. 213-241, 2001.

[13] J. Roenby, H. Bredmose, and H. Jasak, "A computational method for sharp interface advection," *R. Soc. open sci.,* vol. 3, p. 160405, 2016.